

Far-field predictions of metamaterials from two-dimensional near-field measurement system

Hui Feng Ma, Tie Jun Cui^{*}, Xin Mi Yang, Wei Xiang Jiang, and Qiang Cheng
State Key Laboratory of Millimeter Waves and Institute of Target
Characteristics and Identification, Southeast University, Nanjing 210096, P. R. China
^{*} Email: hfma@emfield.org and tjcui@seu.edu.cn

Abstract: In this paper, the near-to-far field transformation is proposed to predict the far fields of metamaterials from the near-field measured data, which can be achieved by two-dimensional (2D) near-field microwave scanning apparatus (2D mapper). The 2D mapper is a near-field scanning system, from which the far-field data cannot be obtained directly. The near-to-far field transformation method has been studied to predict the far fields from the known near-field information, which will make the 2D mapper more efficient in the measurement of metamaterials. The correctness and feasibility of the proposed transformation are verified by both numerical simulations and experiments.

Keywords: Metamaterials, near-field scanning system, far-field prediction

doi: [10.11906/TST.074-084.2010.06.07](https://doi.org/10.11906/TST.074-084.2010.06.07)

1. Introduction

In the past a few years, metamaterials have been achieved great developments and attractions. In the early time, people have committed to the theoretical study of metamaterials, and some exciting results have been obtained [1, 2]. As the development of metamaterials, the pure theoretical study was insufficient for the research of metamaterials, and then great efforts have been made to find structures to construct metamaterials. For example, the metal wires [3], split-ring resonators (SRR) [4], electric inductive-capacitive (ELC) resonators [5], and some other structures [6, 7] of periodic configurations were introduced to achieve metamaterials, which can be treated as the effective artificial media. The effective medium parameters such as permittivity and permeability of an artificially-structured metamaterial can be retrieved from the full-wave electromagnetic simulations [8, 9], and a series of interesting results were obtained from the above structures [10, 11]. Nowadays, the main method to confirm the properties of metamaterials is that we compare the measured transmission, reflection, and scattering properties with the effective medium simulations. Some measurement methods have been introduced in Refs. [12]-[14]. However, only the near fields of metamaterials can be obtained by the two-dimensional (2D) measurement apparatus (2D Mapper). It is difficult to get the far-field information due to the restrictions of the measurement instruments.

The near-to-far field transformation is an effective method in the compact-range measurements of antennas scatterers, which can obtain the far fields an antenna or a target from the three-dimensional measured near-field data [15-18]. The conventional methods to analyze the near-to-far field transformation include the modal expansion and the integral equation approaches [17]. The veracity of such methods has been verified [15-18]. The idea of near-to-far field transformation is very useful for the metamaterial study.

In this paper, we propose the near-to-far field transformation in two dimensions. Such a

method is used to predict the far fields of metamaterials from the near-field measured data, which can be achieved by the 2D near-field microwave scanning apparatus (2D mapper). The 2D mapper is a near-field scanning system, from which the far-field data cannot be obtained directly [12-14]. Hence the proposed method will make the 2D mapper more efficient in the measurement of metamaterials. The correctness and feasibility of the proposed transformation are verified by both numerical simulations and experiments.

2. Theory of near-to-far field transformation

We use the effective magnetic current method to realize the near-field to far-field transformation. Such a method utilizes the measured near-field data to reconstruct the equivalent magnetic current sources over a virtual surface which encompasses the metamaterial target. Once the equivalent magnetic current sources are determined, the near fields outside of the virtual surface and the far fields can be obtained.

Consider a 2D arbitrarily-shaped metamaterial target, as shown in Fig. 1(a). A virtual surface S1, which is a circle with radius R_s , encompasses the target. We assume that S2 is the near-field detection circle with radius R_m . We use the measured near-field data over S2 to determine the equivalent magnetic current \bar{M} over S1. Once the equivalent magnetic current is determined, then the near fields and far fields of the metamaterial target will be obtained. Based on the Huygens' principle, the electromagnetic wave outside S1 can be determined by the equivalent magnetic current sources over S1. From the Maxwell's equations, the electric field generated by a magnetic current source in a homogenous medium is expressed as

$$\bar{E}(\bar{M}) = -\frac{1}{\epsilon_0} \nabla \times \bar{A}_e \tag{1}$$

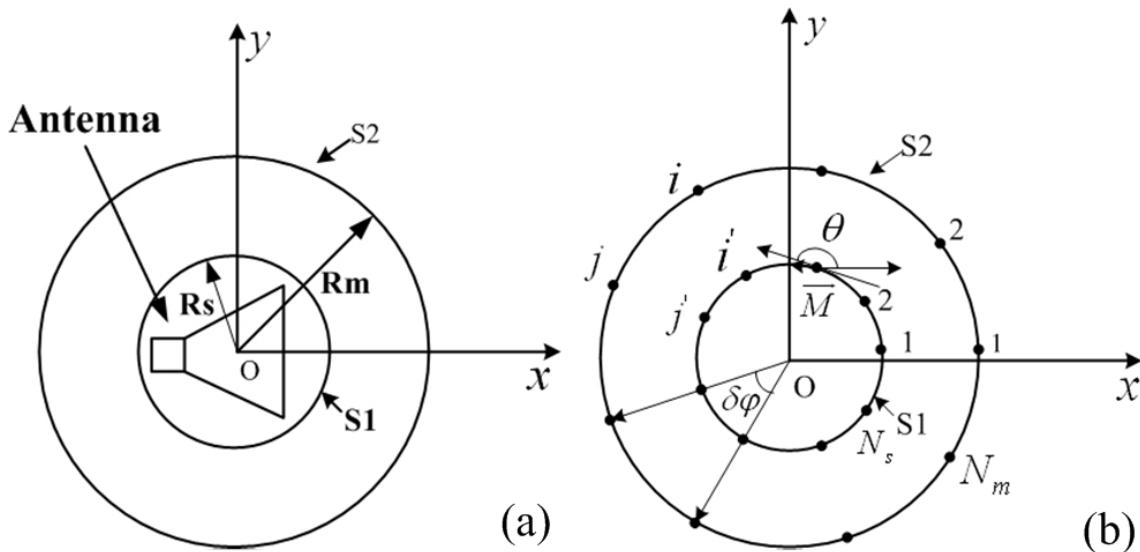


Fig. 1 The equivalent problem with an equivalent magnetic current source, in which S1 is the virtual surface for the equivalent magnetic current and S2 is the near-field detection surface. (a) Equivalent model. (b) The discretization of the equivalent model.

where \bar{A}_e is the electric vector potential defined as

$$\bar{A}_e = \varepsilon_0 \int_{S_1} \bar{M}(\bar{\rho}') g(\bar{\rho}, \bar{\rho}') dl', \quad (2)$$

in which

$$g(\bar{\rho}, \bar{\rho}') = -\frac{j}{4} H_0^{(2)}(k_0 |\bar{\rho} - \bar{\rho}'|), \quad (3)$$

k_0 is the wave number in free space, and

$$\nabla = \hat{x} \frac{\partial}{\partial x} + \hat{y} \frac{\partial}{\partial y}. \quad (4)$$

The method of moment (MOM) has been applied to calculate the effective magnetic current. We divide the near-field detection surface S2 into N_m elements equally. Hence the sampling length of each element is $\delta l_m = Rm \cdot \delta\varphi$, in which $\delta\varphi = 2\pi/N_m$. The effective magnetic current surface S1 is also divided into N_s elements equally ($N_s = N_m$), and the sampling length is $\delta l_s = Rs \cdot \delta\varphi$, as shown in Fig. 1(b). In the engineering applications, the maximum sampling length $(\delta l_m)_{\max} = \lambda_0/2$ can be obtained by the sampling theory [20]. Hence the electric field in the j' -th element of S2 generated by the i -th effective magnetic current element of S1 can be calculated by using Eqs. (1)-(4).

The electric vector potential \bar{A}_{eij} can be obtained from Eq. (2)

$$\bar{A}_{eij} = -I \varepsilon_0 M_i H_0^2(k_0 \rho_{ij}) (\hat{x} \cos \theta_i + \hat{y} \sin \theta_i), \quad (5)$$

in which $\rho_{ij} = \sqrt{(x'_j - x_i)^2 + (y'_j - y_i)^2}$ is the distance between the i -th effective magnetic current element and the j' -th electric-field sampling point, and (x_i, y_i) and (x'_j, y'_j) are the corresponding coordinates. $I = j0.5x_0 \left[1 - (k_0 x_0)^2/12 + (k_0 x_0)^4/320 \right]$, in which $x_0 = \delta l_s/2$. θ_i is the angle between \bar{M}_i and the x axes. Substituting Eq. (5) into Eq. (1), the j' -th electric field on S2 generated by the i -th effective magnetic current element will be achieved as

$$\bar{E}_{ij} = \hat{z} M_i I \frac{k_0}{\rho_{ij}} H_1^{(2)}(k_0 \rho_{ij}) (y_{ij}' \cos \theta_i - x_{ij}' \sin \theta_i). \quad (6)$$

in which $x_{ij}' = x'_j - x_i$ and $y_{ij}' = y'_j - y_i$. Hence the total electric field in j' -th sampling point is obtained

$$E_j = \sum_1^{N_s} M_i I \frac{k_0}{\rho_{ij}'} H_1^{(2)}(k_0 \rho_{ij}') (y_{ij}' \cos \theta_i - x_{ij}' \sin \theta_i). \quad (7)$$

From Eq. (7), a matrix equation on the unknown magnetic current \mathbf{M} can be set up

$$\mathbf{Z} \bullet \mathbf{M} = \mathbf{E}, \quad (8)$$

where

$$Z_{ij} = I \frac{k_0}{\rho_{ij}} H_1^{(2)}(k_0 \rho_{ij}) (y_{ij} \cos \theta_i - x_{ij} \sin \theta_i). \quad (9)$$

Hence we can determine the equivalent magnetic current sources over S1 using the measured near-field data over S2 from Eq. (8), and the electromagnetic fields outside S1 can be then obtained by the equivalent magnetic current sources over S1.

When $\rho \gg x_i, y_j$, the Hankel function can be considered by its large-argument approximation

$$H_0^{(2)}(k_0 |\bar{\rho} - \bar{\rho}'|) \approx \sqrt{\frac{2}{\pi k_0 \rho}} e^{-j\frac{\pi}{4}} e^{jk_0(x_i \cos \phi + y_j \sin \phi)}. \quad (10)$$

Then the radiation electric field can be obtained from Eqs. (1) and (2) with the known effective magnetic current \bar{M} :

$$\bar{E}(\rho, \phi) = -\hat{z} I \sqrt{\frac{2j}{\pi k_0 \rho}} j k_0 e^{-jk_0 \rho} \sum M_i (\sin \theta_i \cos \phi - \cos \theta_i \sin \phi) e^{jk_0(x_i \cos \phi + y_j \sin \phi)}. \quad (11)$$

From Eq. (10), the function of the far-field radiation pattern for the metamaterial target can be expressed as

$$F(\phi) = \sum M_i (\sin \theta_i \cos \phi - \cos \theta_i \sin \phi) e^{jk_0(x_i \cos \phi + y_j \sin \phi)}. \quad (12)$$

where ϕ is the angle between the far-field vector and the x axis.

3. Experimental and numerical results

In this section, we will verify the correctness and accuracy of the proposed near-to-far field transformation for the metamaterial 2D Mapper system. First, we consider an antenna array composed of two infinite-long current filaments, which has closed-form solutions for both near and far fields. The two currents have the same magnitude but opposite phases, whose working frequency is 7.5 GHz . The distance between the two sources is $\lambda/2 = 0.02 \text{ m}$. Fig. 2 shows the full-wave simulation results of the electric field distribution in the near-field region based on the finite element method (FEM), in which the current amplitude is set as $I = 0.001 \text{ A}$ and the two 2D current sources are located at the points $(0, 0.01) \text{ m}$ and $(0, -0.01) \text{ m}$, respectively. The corresponding measurement results using the 2D Mapper are shown in Fig. 3. Because of the singularity, the fields near to the dipole source are so strong that the field distribution in the other region cannot be displayed clearly. Hence the field around the source is not plotted here.

The measurement system is a parallel-plate waveguide apparatus in the X band frequency, as shown in Fig. 4. The top and the bottom plates are both aluminums to serve as perfectly electric conductors (PEC), and the distance between two plates is 13 mm . In the actual measurement

process, the 2D line source (a dipole antenna) is located at the point $(0, 0.01) m$, and an aluminum sheet is placed along the line $y=0 m$ as a PEC plane. The measured electric field distribution is shown in Fig. 3(a). From the image theory, we may replace the PEC sheet with an image source located at the point $(0, -0.01) m$, which has the same magnitude and opposite phase to the original source. Hence the 2D line source and the PEC plane in the measurement system is equivalent to the two-element antenna array mentioned earlier, which should have the same properties compared to the simulation one in Fig. 2. The experimental result of the electric field distribution after using the image theory is illustrated in Fig. 3(b). Comparing Figs. 2 and 3(b), the simulation and experiment results have good agreements, which show good correctness and accuracy of the proposed method.

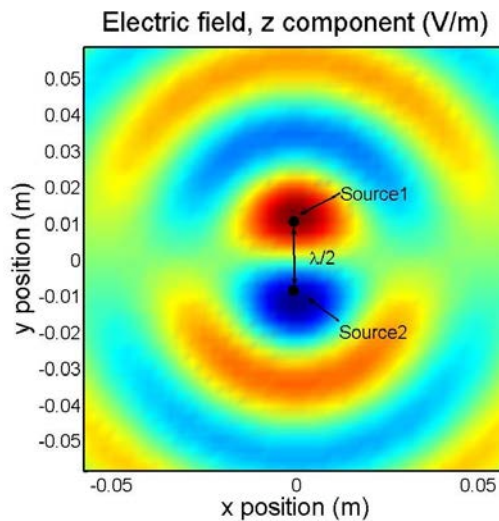


Fig. 2 The full-wave simulation result of near-field distribution for the two-element currents based on the FEM method.

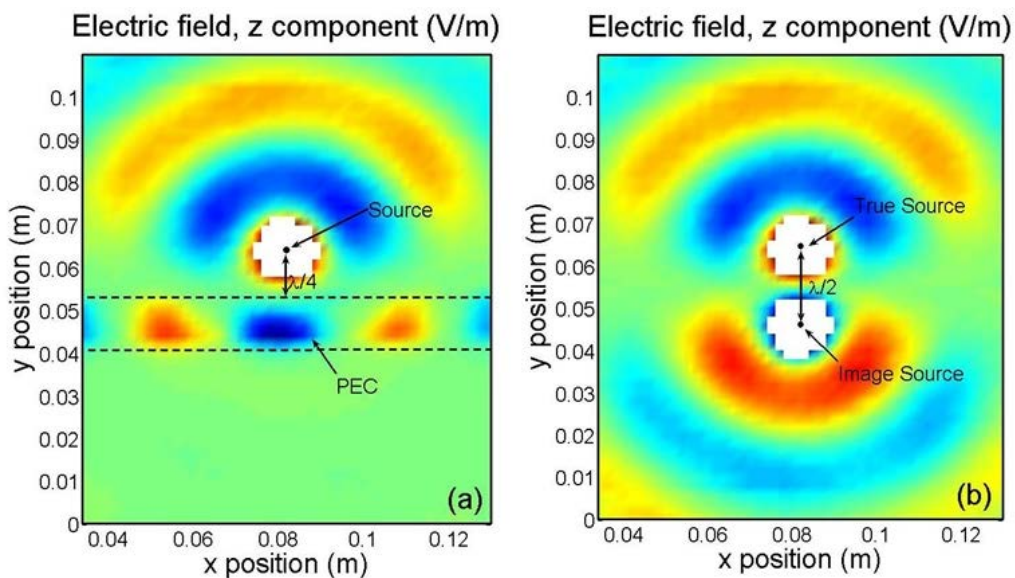


Fig. 3 The measurement results of near-field distributions. (a) The direct measurement result for single current source and a PEC plane. (b) The expanded measurement result for two current sources based on the image theory.



Fig. 4 The 2D near-field microwave scanning apparatus to measure the near fields shown in Fig. 2.

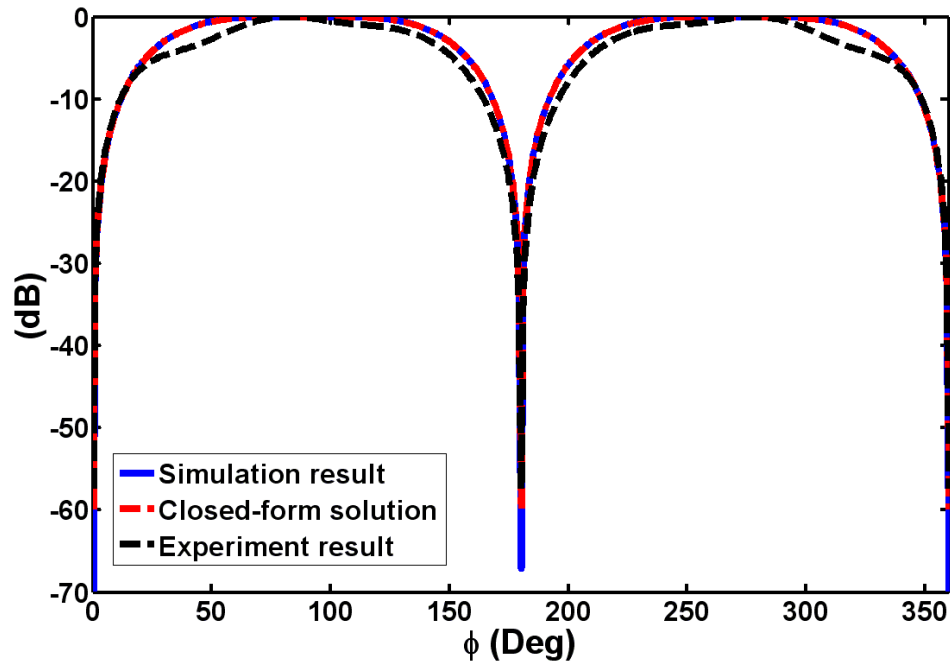


Fig. 5 The far-field radiation patterns of the two-element current array: a comparison among the near-to-far field transformation results (both simulation and measurement) and the closed-form solution.

The far-field radiation patterns from the near-to-far field transformation using the measured near-field data and simulated near-field data, respectively, and from the closed-form solution are demonstrated in Fig. 5. From Fig. 5, we clearly see that the analytical result has a perfect match to the near-to-far field transformation using the simulation data, which are nearly the same. Both results have good agreement to the near-to-far field transformation using the measured data. Hence the proposed near-to-far field transformation method is accurate to predict the far fields for the 2D mapper.

To further validate the accuracy of the proposed near-to-far field transformation for the 2D Mapper, we then apply the method to calculate the scattering width of a 2D dielectric cylinder. The circular dielectric cylinder has a radius of $R=0.3\lambda$, which is illuminated by TM waves with unit amplitude of electric field. The incident waves are z -direction polarized and propagate along the x direction. The parameters of the dielectric cylinder are $\epsilon_r=4$ and $\mu_r=1$. Fig. 6 shows the full-wave simulation results using the FEM method, in which the total and scattered electric fields are demonstrated in Figs. 6(a) and 6(b), respectively.

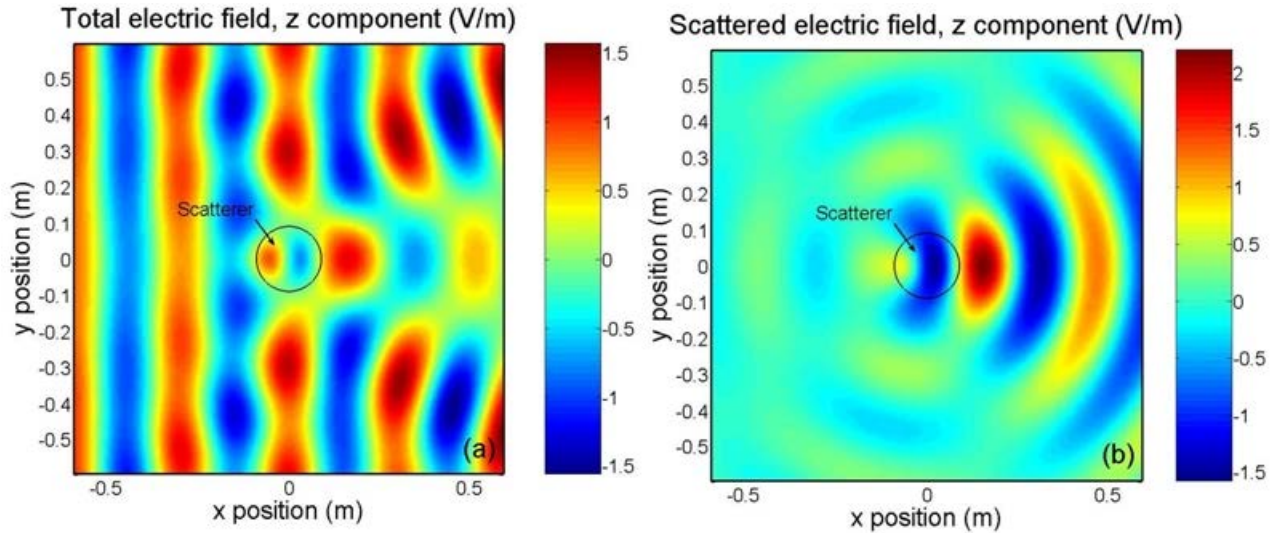


Fig. 6 The near-electric-field distributions of the 2D dielectric cylinder illuminated by the TM-polarized plane waves. (a) The total electric field. (b) The scattered electric field.

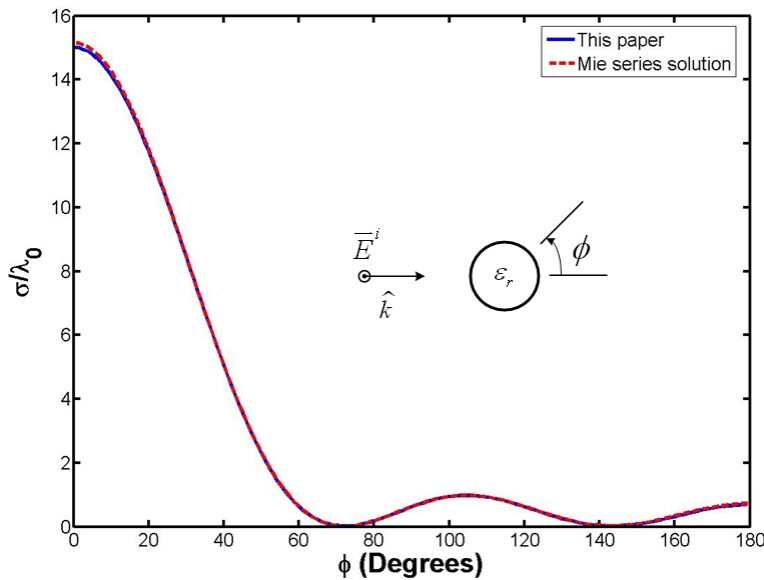


Fig. 7 The scattering width of the dielectric cylinder illuminated by the TM-polarized plane waves.

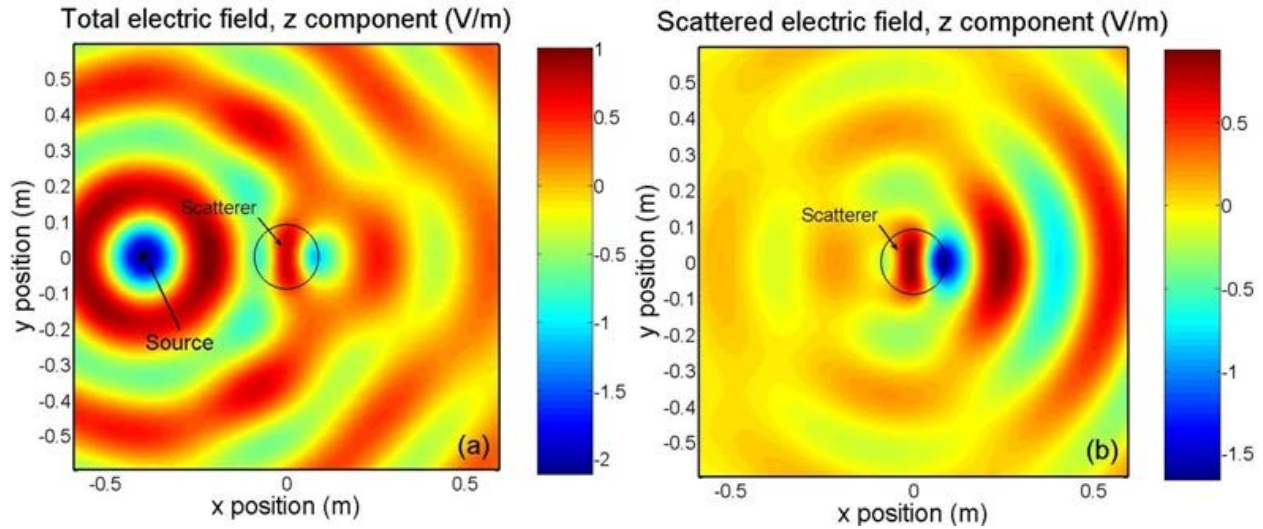


Fig. 8 The near-electric-field distributions of the 2D dielectric cylinder illuminated by the line source. (a) The total electric field. (b) The scattered electric field.

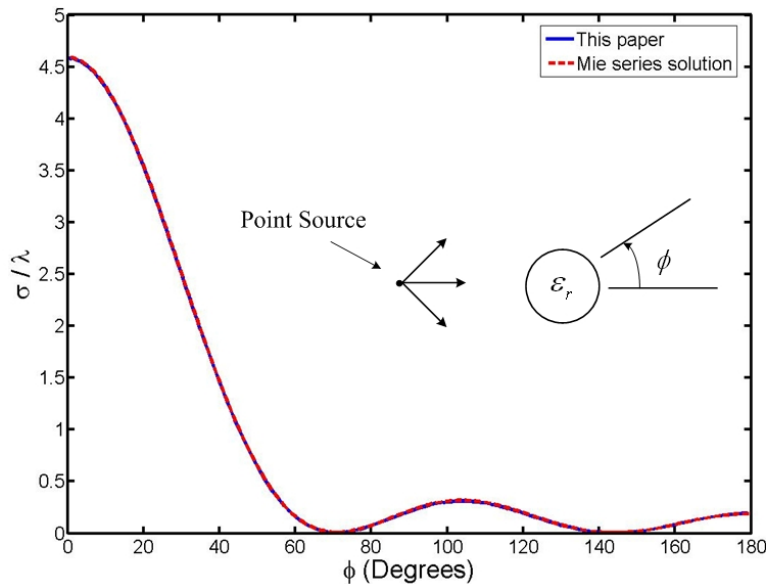


Fig. 9 The scattering width of the dielectric cylinder illuminated by the line source.

Now we apply the near scattered fields to generate the effective magnetic sources around the scatterer. Based on the near-to-far field transformation, the far-field scattering width of the dielectric cylinder has been computed, as shown in Fig. 7. As a comparison, a direct computation of the scattering width is also conducted using the Mie series solution, as illustrated in Fig. 7. For the same dielectric cylinder, under the excitation of a 2D line source, the full-wave simulation results of near-field distributions based on FEM are demonstrated in Fig. 8. Using the near-to-far field transformation, the far-field scattering width is calculated, as shown in Fig. 9. Again, a direct computation of the scattering width using the Mie series is also given for comparison. From Figs. 7 and 9, the two results have perfect match in both excitations, which verify the accuracy of the proposed near-to-far field transformation for the 2D Mapper.

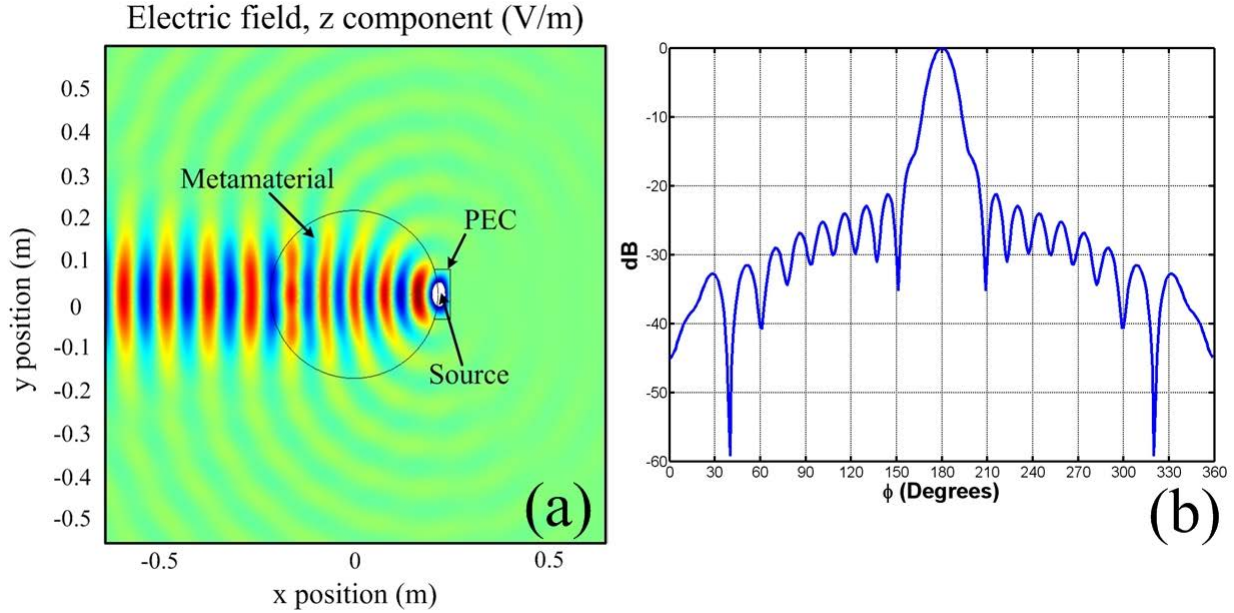


Fig. 10 The gradient-index metamaterial lens antenna. (a) The full-wave simulation result of near field using FEM. (b) The far-field radiation pattern of the antenna.

Finally, we design a metamaterial lens antenna, which is similar to a Luneberg antenna [19]. The lens has the circular symmetrical configuration, whose radius is $R=0.2\text{ m}$, and the corresponding simulation result using FEM are illustrated in Fig. 10(a). In the antenna model, the line source is located at the edge of the circular lens. The parameter distributions are given by $\varepsilon_r=2-r/R$ and $\mu_r=1$, in which $0<r<R$. The current of excitation is $I=0.001\text{ A}$ at the frequency of 3 GHz . From Fig. 10(a), we clearly see that the cylindrical waves emitted from the line source are quickly transformed the plane waves, which can be used as high-gain antenna. Based on the near-field distribution, the far-field radiation pattern of the metamaterial antenna is predicted using the proposed method, as shown in Fig. 10(b). Clearly, the antenna has a very good performance with high gain and low sidelobes.

5. Conclusions

In this paper, we propose a near-to-far field transformation to predict the far fields of metamaterials using the simulation or measurement near-field results from the 2D mapper system. The correctness and accuracy of the proposed transformation are verified by both numerical simulations and experiments.

Acknowledgment

This work was supported in part by the National Science Foundation of China under Grant Nos. 60871016, 60671015, 60601002, and 60621002, in part by the Natural Science Foundation of Jiangsu Province under Grant No. BK2008031, in part by the National Basic Research Program (973) of China under Grant No. 2004CB719802, and in part by the 111 Project under Grant No.

111-2-05.

References

- [1] V. G. Veselago, The electrodynamics of substances with simultaneously negative values of ϵ and μ . *Sov. Phys.-Usp.*, 10, 509-514, (1968).
- [2] J. B. Pendry, Negative Refraction Makes a Perfect Lens, *Phys. Rev. Lett.*, 85, 3966-3969, (2000).
- [3] J. B. Pendry, A. J. Holden, W. J. Stewart, and I. Youngs, Extremely low frequency plasmons in metallic mesostructures, *Phys. Rev. Lett.*, 76, 4773-4776, (1996).
- [4] J. B. Pendry, A. J. Holden, D. J. Robbins, and W. J. Stewart, Magnetism from conductors and enhanced nonlinear phenomena, *IEEE Trans. Microwave Theory Tech.*, 47, 2075-2084, (1999).
- [5] D. Schurig, J. J. Mock, and D. R. Smith. Electric-field-coupled resonators for negative permittivity metamaterials, *Appl. Phys. Lett.*, 88, 041109, (2006).
- [6] R. Marque's, F. Mesa, J. Martel, and F. Medina, Comparative analysis of edge- and broadside-coupled split ring resonators for metamaterial design – theory and experiments, *IEEE Trans. Antennas Propag.*, 51, 2572–2581, (2003).
- [7] F. Falcone, T. Lopetegui, M. A. G. Laso, J. D. Baena, J. Bonache, M. Beruete, Babinet Principle Applied to the Design of Metasurfaces and Metamaterials, *Phys. Rev. Lett.*, 93, 197401, (2004).
- [8] X. D. Chen, Bae-Ian Wu, Jin Au Kong, and Tomasz M. Grzegorzcyk, Retrieval of the effective constitutive parameters of bianisotropic metamaterials, *Phys. Rev. E.*, 71, 046610, (2005).
- [9] L. L. Hou, J. Y. Chin, X. M. Yang, X. Q. Lin, R. Liu, F. Y. Xu, T. J. Cui, Advanced parameter retrievals for metamaterial slabs using an inhomogeneous model, *J. Appl. Phys.*, 103, 064904, (2008).
- [10] R. Shelby, D. R. Smith, and S. Schultz, Experimental verification of a negative index of refraction, *Science*, 292, 77-79, (2001).
- [11] D. Schurig, J. J. Mock, B. J. Justice, S. A. Cummer, J. B. Pendry, A. F. Starr, D. R. Smith, Metamaterial Electromagnetic Cloak at Microwave Frequencies, *Science*, 1133628, 1-4, (2006).
- [12] B. I. Popa and S. A. Cummer, Wave fields measured inside a negative refractive index metamaterial, *Appl. Phys. Lett.*, 85, 4564-4566, (2004).
- [13] B. I. Popa and S. A. Cummer, Direct measurement of evanescent wave enhancement inside passive metamaterials, *Phys. Rev. E.*, 73, 016617, (2006).
- [14] Bryan J. Justice, Jack J. Mock, Liheng Guo, Aloyse Degiron, David Schurig, and David R. Smith, Spatial mapping of the internal and external electromagnetic fields of negative index metamaterials, *Opt. express*, 16, 8694-8705, (2006).
- [15] Peter Petre and Tapan K. Sarkar, Planar Near-Field to Far-Field Transformation Using an Equivalent Magnetic Current Approach, *IEEE Trans. Antennas Propagat.*, 40, 1348-1356, (1992).
- [16] Peter Petre and Tapan K. Sarkar, Planar near field to far field transformation using an array and dipole probes, *IEEE Trans. Antennas Propagat.*, 42, 534-537, (1994).
- [17] Peter Petre and Tapan K. Sarkar, Difference between modal expansion and integral equation methods for planar near-field to far-field transformation, *PIER*, 12, 37-56, (1996).

- [18] Tapan Kumar Sarkar, and Ardalan Taaghola, Near-Field to Near/Far-Field Transformation for Arbitrary Near-Field Geometry Utilizing an Equivalent Electric Current and MoM, *IEEE Trans. Antennas Propagat.*, 47, 566-573, (1999).
- [19] R. K. Luneberg, *Mathematical Theory of Optics*, Brown University Press, Providence, R. I., (1944).